Monthly Notices
of the
ROYAL ASTRONOMICAL SOCIETY

MNRAS **460,** 1640–1644 (2016)
Advance Access publication 2016 April 29

doi:10.1093/mnras/stw1012

Discovery of a deep Seyfert-2 galaxy at $z = 0.222$ behind NGC 300

J. A. Combi,[1,2★] F. García,[1,2★] M. J. Rodríguez,[3★] R. Gamen[2,3] and S. A. Cellone[2,3]

[1]*Instituto Argentino de Radioastronomía (CCT La Plata, CONICET), C.C.5, (1894) Villa Elisa, Buenos Aires, Argentina*
[2]*Facultad de Ciencias Astronómicas y Geofísicas, Universidad Nacional de La Plata, Paseo del Bosque, B1900FWA La Plata, Argentina*
[3]*Instituto de Astrofísica de La Plata, (CCT La Plata, CONICET, UNLP), Paseo del Bosque, B1900FWA, La Plata, Argentina*

Accepted 2016 April 25. Received 2016 April 25; in original form 2016 March 19

ABSTRACT

We report on the unveiling of the nature of the unidentified X-ray source 3XMM J005450.3–373849 as a Seyfert-2 galaxy located behind the spiral galaxy NGC 300 using *Hubble Space Telescope* data, new spectroscopic Gemini observations and available *XMM–Newton* and *Chandra* data. We show that the X-ray source is positionally coincident with an extended optical source, composed of a marginally resolved nucleus/bulge, surrounded by an elliptical disc-like feature and two symmetrical outer rings. The optical spectrum is typical of a Seyfert-2 galaxy redshifted to $z = 0.222 \pm 0.001$, which confirms that the source is not physically related to NGC 300. At this redshift the source would be located at 909 ± 4 Mpc (comoving distance in the standard model). The X-ray spectra of the source are well fitted by an absorbed power-law model. By tying $N_{\rm H}$ between the six available spectra, we found a variable index Γ running from ∼2 in 2000–2001 to 1.4–1.6 in the 2005–2014 period. Alternatively, by tying Γ, we found variable absorption columns of $N_{\rm H} \sim 0.34 \times 10^{-22}$ cm^{-2} in 2000–2001, and $0.54-0.75 \times 10^{-22}$ cm^{-2} in the 2005–2014 period. Although we cannot distinguish between a spectral or absorption origin, from the derived unabsorbed X-ray fluxes, we are able to assure the presence of long-term X-ray variability. Furthermore, the unabsorbed X-ray luminosities of $0.8–2 \times 10^{43}$ erg s^{-1} derived in the X-ray band are in agreement with a weakly obscured Seyfert-2 AGN at $z \approx 0.22$.

Key words: galaxies: Seyfert – X-rays: galaxies – X-rays: individual: 3XMM J005450.3–373849 — X-rays: individual: XMMU J005450.0–373853.

1 INTRODUCTION

Unidentified extragalactic variable X-ray sources with extended emission at radio and optical wavelengths are often associated with active galactic nuclei (AGNs; Mushotzky, Done & Pounds 1993) or Ultraluminous X-ray sources (ULXs; e.g. Fabbiano 2006). Multiwavelength analyses, from radio to gamma-ray, are needed to disentangle and characterize the different components and nature of such astrophysical systems.

Of particular interest is the X-ray source 3XMM J005450.3−373849, located within the spiral galaxy NGC 300, belonging to the nearby Sculptor Group of galaxies. It was first studied by Read & Pietsch (2001), who suggested an X-ray binary nature for the source, based on hardness-ratio values and its variable behaviour obtained from observations performed with the High Resolution Imager of *ROSAT*. Later on, Payne et al. (2004) showed that the source (named XMM5 in their work) presents a radio counterpart (ATCA J005450.3−373850), whose extended radio emission may be the result of synchrotron radiation from jets, possibly associated with an extragalactic microquasar. A study of the global properties of X-ray point sources in NGC 300, and their optical counterparts, was performed by Carpano et al. (2005), who associated the source (named Source 7 in their work) with an apparently extended optical counterpart.

In this paper, we report results of a combined optical and X-ray analysis using archival data of the *Hubble Space Telescope* (*HST*), *XMM–Newton* and *Chandra* observatories, together with new optical spectroscopic *Gemini* observations, of the extragalactic X-ray source 3XMM J005450.3−373849, and we provide convincing evidence about its true nature as a Seyfert-2 AGN galaxy located at $z = 0.222$. The structure of the paper is as follows: in Section 2 we describe *Hubble*, *Gemini*, *XMM–Newton* and *Chandra* observations and data reduction. Optical/X-ray analysis and results are shown in Section 3. Finally, in Section 4, we discuss the implications of our results and summarize our main conclusions.

2 OBSERVATIONS AND DATA REDUCTION

2.1 X-ray data

We analysed four *XMM–Newton* and two *Chandra* observations of 3XMM J005450.3−373849 obtained along a period of 14 years

★ E-mail: jorgearielcombi@gmail.com (JAC); fgarcia@fcaglp.unlp.edu.ar (FG); jimirod@gmail.com (MJR)

Table 1. *Chandra* and *XMM–Newton* observations of 3XMM J005450.3–373849.

Obs.	Satellite	Observation ID	Date	Starting time	Exposure [ks] MOS1/MOS2/pn	GTI [ks]	Observation mode
1	*XMM*	0112800201	2000-12-26	18:14:32	33.7/33.7/28.3	32.3/31.9/24.5	PFWE
2	*XMM*	0112800101	2001-01-01	13:06:32	43.4/43.4/34.6	42.9/43.1/34.4	PFWE
3	*XMM*	0305860301	2005-11-25	07:20:47	36.0/36.0/30.8	35.6/35.9/30.5	PFWE
4	*XMM*	0656780401	2010-05-28	13:23:23	17.8/17.8/11.8	13.9/14.6/10.9	PFWE
5	*Chandra*	12238	2010-09-24	02:57:22	65.80	62.9	VFAINT
6	*Chandra*	16028	2014-05-16	19:33:04	65.08	64.2	VFAINT

Note. All observations were taken from their respective mission archives. PFWE refers to the Prime Full Window Extended observation mode, and VFAINT to very faint mode.

between 2000/12/26 and 2014/05/16. The *XMM–Newton* observations were performed with the European Photon Imaging Camera (EPIC), which consists of three detectors, two MOS cameras (Turner et al. 2001), and one PN camera (Strüder et al. 2001) operating in the 0.2−15 keV range. *XMM–Newton* data were analysed with the *XMM–Newton* Science Analysis System (SAS) version 14.0.0. Starting from level-1 event files, the latest calibrations were applied with the EMPROC and EPPROC tasks. For the MOS data, we selected only events with patterns 0 through 12 and applied flag filters XMMEA_EM. For the PN data, we selected only events with patterns 0 through 4 and applied flag filters XMMEA_EP. According to the light curves of MOS and PN cameras, we further excluded time-intervals with high background rates by setting good time interval (GTI) thresholds on 0.35 count s^{-1} in the 0.3−12 keV range for MOS and 0.4 count s^{-1} in the 0.3−15 keV range for PN, respectively.

Chandra observations performed with the Advanced CCD Image Spectrometer (ACIS) camera were extracted from the archive. ACIS operates in the 0.1–10 keV range with high spatial resolution (0.5 arcsec). These observations were calibrated using the CIAO (version 4.7) and CALDB (version 4.6.7) packages by means of the CHANDRA_REPRO task. Detailed information about the X-ray observations and instrumental characteristics is given in Table 1.

2.2 Optical data

In order to analyse the properties of the optical counterpart of 3XMM J005450.3−373849, found by Carpano et al. (2005), we used optical images obtained with the Advanced Camera for Surveys (ACS) mounted in the *HST*. The observations correspond to the *HST* Cycle 11, and were obtained as part of the GO-9492 program (PI: F. Bresolin) from 2002 July to 2002 December. Three exposures of 360 s are available, performed in the *F435W*, *F555W* and *F814W* filters (Bresolin et al. 2005), which are similar to the classical Johnson *BVI* bands. The ACS Wide Field Camera (WFC) has a mosaic of two CCDs detectors of 4096 × 2048 pixels and a scale of 0.049 arcsec $pixel^{-1}$, covering a field of 3.3 × 3.3 $arcmin^2$. These images and their corresponding photometric data (Dalcanton et al. 2009) were obtained from the Space Telescope Science Institute (STScI) (MAST; https://archive.stsci.edu/) data base. The photometry was carried out using the package DOLPHOT adapted for the ACS camera (Dolphin 2000).

2.3 Gemini spectroscopy

Spectra for 3XMM J005450.3−373849 were taken with the Gemini MultiObject Spectrograph (GMOS) at the Gemini South telescope under the programme GS-2015B-DD-6 (PI: J. Combi).

We have adopted a single long-slit of width 0.75 arcsec to obtain the spectra of the target. We used the R400_G5325 grism and obtained five exposures of 1200 s in two different central wavelengths (three in 6700 Å and two in 6500 Å). This setup resulted in a spectral coverage of 4200–9050 Å and a resolution [defined as λ/full width at half-maximum (FWHM) measured in some emission lines of the CuAr arc lamps spectra] $R \sim 1300$.

The flat-field frames were observed at the same position of the target. The CuAr arc lamps were observed as day-time calibrations, thus flexures can introduce some systematic uncertainties in the wavelength calibration which are not important to the aims of this work. The observations were reduced using the GEMINI package within IRAF.[1]

3 RESULTS

3.1 X-ray spectral and temporal analysis

We checked the position of 3XMM J005450.3−373849 in *Chandra* observations running the WAVDETECT task which had $\alpha = 00^h\,54^m\,50\overset{s}{.}2$ and $\delta = -37^\circ\,38'\,50\overset{''}{.}6$ (J2000.0) with a positional uncertainty of 0.75 arcsec. This value agrees very well with the values reported by Rosen et al. (2015) on their 3XMM-DR5 catalogue: $\alpha = 00^h\,54^m\,50\overset{s}{.}3$ and $\delta = -37^\circ\,38'\,49\overset{''}{.}5$ (J2000.0) with a 0.8 arcsec position error. We also used the SRCEXTENT CIAO task to calculate the size of the source, which resulted point-like, or unresolved, at *Chandra* resolution.

In order to analyse the physical properties of the X-ray emission detected from 3XMM J005450.3−373849 in detail, we extracted spectra from circular regions centred at the position of the source for both *XMM–Newton* and *Chandra* observations. For *XMM–Newton* data, spectra were obtained in the 0.5–12 keV energy range, for radii of 15 arcsec using EVSELECT SAS task with the appropriate parameters for EPIC MOS 1/2 and PN cameras, and ancillary and response matrices were created using ARFGEN and RMFGEN tasks, respectively. For the spectral extraction in MOS1/2 and PN cameras we selected events with FLAG = 0. In the case of *Chandra* data, we extracted spectra using radii of 2 arcsec by means of the SPECEXTRACT CIAO task. For both telescopes, background spectra were extracted from annuli regions centred at the position of the source and the spectra were grouped with a minimum of 16 counts per bin. Spectral analysis was performed using the XSPEC package version 12.8 (Arnaud 1996) in the 0.5–8.0 keV energy range, where the source is detected.

We simultaneously fitted the spectra obtained with the *XMM–Newton* and *Chandra* detectors, using a power-law (PL) model modified by interstellar absorption (PHABS; Balucinska-Church &

[1] http://iraf.noao.edu/

Table 2. Spectral parameters of 3XMM J005450.3–373849.

Obs.	N_H [10^{22} cm^{-2}]	Γ	Flux (0.5–8.0 keV)
	Model I		
1	0.40 ± 0.03	2.06 ± 0.08	0.145 ± 0.006
2	†	1.97 ± 0.08	0.120 ± 0.004
3	†	1.65 ± 0.12	0.057 ± 0.004
4	†	1.48 ± 0.13	0.066 ± 0.004
5	†	1.51 ± 0.11	0.111 ± 0.006
6	†	1.49 ± 0.12	0.102 ± 0.006
χ^2	216.18 (226 d.o.f)		
	Model II		
1	0.33 ± 0.03	1.89 ± 0.06	0.138 ± 0.006
2	0.36 ± 0.03	†	0.116 ± 0.005
3	0.54 ± 0.09	†	0.062 ± 0.006
4	0.66 ± 0.11	†	0.076 ± 0.007
5	0.60 ± 0.10	†	0.119 ± 0.009
6	0.75 ± 0.14	†	0.121 ± 0.011
χ^2	229.67 (226 d.o.f)		

Notes. Error values are 1σ (68 per cent) for every single parameter and unabsorbed fluxes in the 0.5–8.0 keV energy range are given in units of 10^{-12} erg cm^{-2} s^{-1}. Parameters indicated with a dagger (†) were tied between each other during the fit. Model I corresponds to values of N_H tied and Model II to values of Γ tied, respectively.

McCammon 1992). In order to fit the data we used to alternatives. In Model I, we tied the hydrogen column density, N_H, of all observations allowing us to vary freely the spectral indices, Γ, and their normalizations, while in Model II, we tied Γ, allowing us to vary the N_H. For Model I, the best-fitting model returned a hydrogen column density $N_H = 0.40 \pm 0.03 \times 10^{22}$ cm^{-2} and PL indices varying from ∼2, for Obs. 1 and 2, to 1.48–1.65 for Obs. 3 to 6, with a total χ^2 of 216.18 for 226 d.o.f. Unabsorbed X-ray fluxes in the 0.5–8.0 keV energy range run from 0.145 to 0.057 × 10^{-12} erg cm^{-2} s^{-1}. For Model II, the best fit corresponds to a spectral index $\Gamma = 1.89 \pm 0.06$, and absorption columns varying from $\sim 0.35 \times 10^{22}$ cm^{-2}, for Obs. 1 and 2, to $0.54-0.75 \times 10^{22}$ cm^{-2}, for Obs. 3 to 6, with a total χ^2 of 229.67 for 226 d.o.f. Unabsorbed X-ray fluxes in the 0.5–8.0 keV range show a similar behaviour to Model I, being the same, regardless of the model chosen. The available data do not allow us to adequately fit the whole set of spectra, leaving all the parameters untied, as there are no enough statistics. However, in both cases we observe the presence of a long-term X-ray variability. The full results of the fits are summarized in Table 2.

On the left panel of Fig. 1 we plot the spectral results corresponding to Model I. On its upper panel, we present the evolution of the spectral index Γ of 3XMM J005450.3−373849 from 2000 December 26 to 2014 May 16. The PL spectral index was ∼2 during the period 2000/2001, decreasing to ∼1.5 in 2005/2014. On its lower panel we show the corresponding full 2000–2014 unabsorbed X-ray light curve in the 0.5–8.0 keV energy range. On the right panel of Fig. 1 we display the spectral results from Model II. On its upper panel, we show the evolution of the absorption column N_H, while on its lower panel we plot the corresponding X-ray light curve in the same ranges. Although a few years of data are missing (2001–2005), in both cases the source displays at least two different states. Regardless of the model chosen, the unabsorbed flux evolution shows the same behaviour which confirms the long-term X-ray variability of the source. To make this clear, in Fig. 2 we show background-subtracted PN spectra of *XMM–Newton* observations 1 and 4 of 3XMM J005450.3−373849 as fitted by the absorbed PL model.

3.2 Optical images and photometry

Fig. 3 shows the *HST* images of the field surrounding 3XMM J005450.3−373849 in the aforementioned three filters. The *Chandra* X-ray contours are overlaid in Fig. 3, left panel. As can be seen, the X-ray source is positionally coincident with the geometrical centre of the extended optical source, whose morphology clearly matches an R'_1-type ring galaxy, in which two outer pseudo-rings are conspicuous. These features are thought to arise from gaseous rings that developed at the outer Lindblad resonances (OLR) in a spiral galaxy (e.g. Buta & Crocker 1991). The optical source also displays a barely resolved nuclear component (which we associate with a bulge plus an unresolved nucleus), located at the centre of an 'oval', with hints of spiral structure, and two 'hot-spots', clearly seen in the *B*-band image at position angles 66° and 238° (i.e. almost at diametrically opposite sides of the nucleus).

The inner disc (the 'oval' feature) has an ellipticity $\epsilon = 0.36$ and a position angle PA ≈ 5°, spanning 0.86 and 0.57 arcsec along its major and minor axes, respectively. The pseudo-rings, in turn, present an angular size of $\sim 3.5 \times 2.5$ arcsec^2 on the plane of the sky.

3.3 Optical spectroscopy

In Fig. 4, we show the GMOS spectrum over the spectral range 5500–8500 Å. Emission lines of H, He I, [N II], [O I–II–III], [S II], [Ar III], and [Fe VII] were identified in the spectrum and measured for radial velocities. We obtained a mean $z = 0.2216 \pm 0.0008$ (13 measurements). We have also identified some absorption lines of Ca II, Na I, and the *G* band. Five absorptions gave a $z = 0.2223 \pm 0.0005$ (five values averaged). Hence, absorptions are originated at the same distance as the emission lines.

The spectrum presents hydrogen and forbidden lines of the same width with a mean FWHM ∼ 500 ± 150 km s^{-1}, compatible with a Seyfert-2 galaxy spectrum. Also, the ratio Hβ and [O III] λ5007 is 0.1 (typical in Sy 2, following Weedman 1977).

We also measured the FWHM of the emission lines in the spatial dimension. All of them were similar to the FWHM of the whole trace of the spectrum, thus the spectral source should be considered as point-like (at least, considering the seeing-limited Gemini's spatial resolution).

4 DISCUSSION

Through this paper, for the first time, we present a deep study of the X-ray source 3XMM J005450.3−373849 and its optical counterpart to unveil its real nature. The information gathered in the previous sections from the optical and X-ray analysis shows that 3XMM J005450.3−373849 possesses typical characteristics of a Seyfert-2 AGN galaxy, located at $z = 0.222 \pm 0.001$ behind NGC 300, as revealed by the optical spectroscopic observations that we obtained with Gemini. The X-ray source is positionally coincident with the central region of an extended optical source detected with *HST* showing a complex structure that clearly matches the morphology of an R'_1-type spiral galaxy with a conspicuous outer pseudo-rings structure. The positional correlation strongly suggests a physical association between both sources. We also note that this galaxy is unrelated to either of the two clusters detected in the background of NGC 300 (Schirmer et al. 2003), with measured redshifts $z = 0.165$

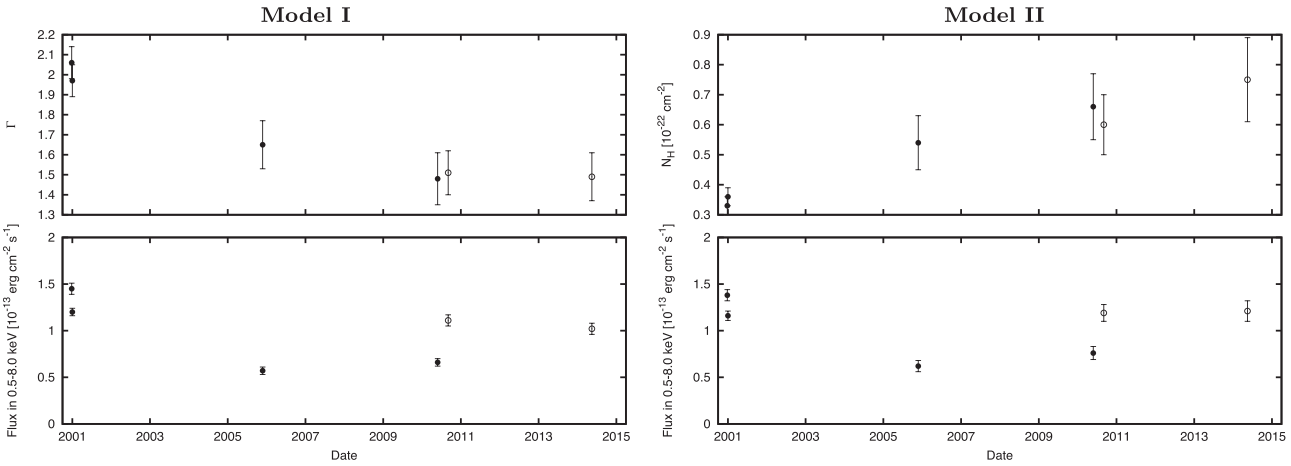

Figure 1. Left panels: spectral results for Model I. Upper panel: spectral index Γ evolution from 2000 Dec 26 to 2014 May 16. Bottom panel: unabsorbed total flux (0.5–8.0 keV) evolution in the same period. Right panels: spectral results for Model II. Upper panel: $N_{\rm H}$ evolution from 2000 Dec 26 to 2014 May 16. Bottom panel: unabsorbed total flux (0.5–8.0 keV) evolution also in the same period. Black and white circles represent *XMM–Newton* and *Chandra* observations, respectively.

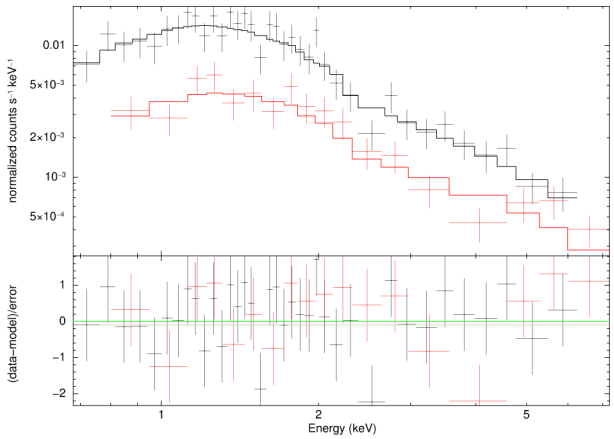

Figure 2. *XMM–Newton* PN spectra of 3XMM J005450.3−373849 obtained from observations 1 (black) and 4 (red). Solid lines represent the best fit using an absorbed PL model (see Table 2). Lower panel shows χ^2 fit residuals. Error bars are at 90 per cent confidence intervals.

(Cappi, Held & Marano 1998) and $z = 0.117$ (Collins et al. 1995), respectively.

The object's redshift implies a luminosity distance $d_{\rm L} = 1111 \pm 6$ Mpc and a spatial scale 3.606 kpc arcsec^{-1} (we made use of Ned Wright's *Cosmology Calculator*,[2] with standard Cosmological parameters: $H_0 = 69.6$ km s^{-1} Mpc^{-1}, $\Omega_{\rm M} = 0.286$, and $\Omega_\Lambda = 0.714$.). The (projected) major axis of the pseudo-rings system is thus ≈12 kpc, while the surface brightness profile of the inner 'oval' feature can be fitted by an exponential with a scale-length of 0.56 ± 0.02 arcsec (2.02 ± 0.06 kpc) in the *I* band (rest-frame *R* band). The rings are resolved into several 'knots' with apparent magnitudes ranging from $V \sim 25$ to $V \sim 27$ mag ($-15.2 \lesssim M_V \lesssim -13.2$) and relatively red colours ($0.0 \lesssim B - V \lesssim 1.5$). Thus, they are probably large star-forming complexes (the Hα emission falls within the F814W passband at the object's redshift), significantly reddened by the intervening dust in the disc of NGC 300.

[2] http://www.astro.ucla.edu/wright/CosmoCalc.html; Wright 2006

Though a small fraction of observed rings may be due to collisions or mergers of galaxies, or to accretion of intergalactic gas, the vast majority of rings are probably simple resonance phenomena, caused by the actions of a rotating bar or other non-axisymmetric disturbance on the motions of gas clouds in the disc (e.g. Schwarz 1981). In particular, outer pseudo-rings are in fact spiral arms with a very low pitch angle, winding upon themselves following the OLR. These features are quite common in Seyfert galaxies (Hunt & Malkan 1999), and it has been suggested that galaxies with outer (pseudo)rings tend to display enhanced nuclear star formation (Buta & Crocker 1991); however, the real dependence of AGN activity on the global structure of the host galaxy is still debated (Cisternas et al. 2015).

The information obtained from the optical data is in accordance with the results of our temporal and spectral X-ray analysis of 3XMM J005450.3−373849, where we have shown that the source was in two different states, showing typical AGN variability. The X-ray spectra available were best fitted using an absorbed PL model, with absorption columns in the 0.33–0.75 × 10^{22} cm^{-2} range and spectral indices of 1.5–2 typical of AGNs. In the 2000–2001 period, the source showed a highest flux, reaching 0.12–0.14 × 10^{-12} erg cm^{-2} s^{-1}. Contrarily, during the 2005–2010 period, the source was fainter with a flux of ∼0.06 × 10^{-12} erg cm^{-2} s^{-1} with a higher absorption, returning to a brighter state in the last 2010–2014 period. Taking into account the derived unabsorbed X-ray fluxes of the source, assuming a 1110 Mpc distance to the source, we compute X-ray luminosities in ∼8 × 10^{42} to 2 × 10^{43} erg s^{-1} range for the 0.5–8.0 keV energy band, for any of the spectral models assumed, which correspond to a weak AGN with little obscuration (Merloni et al. 2014; Ueda et al. 2014). It is interesting to note that considering an $E(B-V) = 0.075$ for NGC 300 (Gieren et al. 2004) and assuming $R = 3.1$, we deduce an $A_V = 0.2325$. Thus, following Foight et al. (2015) we obtain a total absorption column $N_{\rm H} = 5 - 7 \times 10^{20}$ cm^{-2}. Hence, the best-fitting values obtained for the absorption columns in both spectral models are at least a factor of 5 higher than the foreground material.

In any case, this particular galaxy has signatures of strong star formation activity, as well as of an AGN. The two hot spots, as said, are prominent in the F435W image (which corresponds to the *U* band at the source rest-frame). Such spots, roughly aligned on

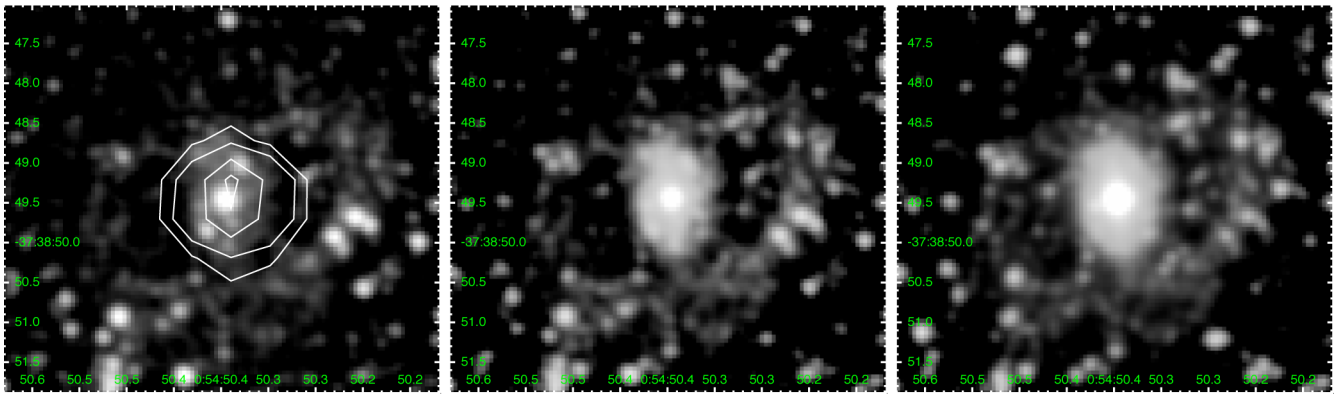

Figure 3. *HST* images of the extended optical source positionally coincident with 3XMM J005450.3−373849. From left to right we show the *F435W*, *F555W* and *F814W* filters. X-ray contours are overlaid in white colour (left panel).

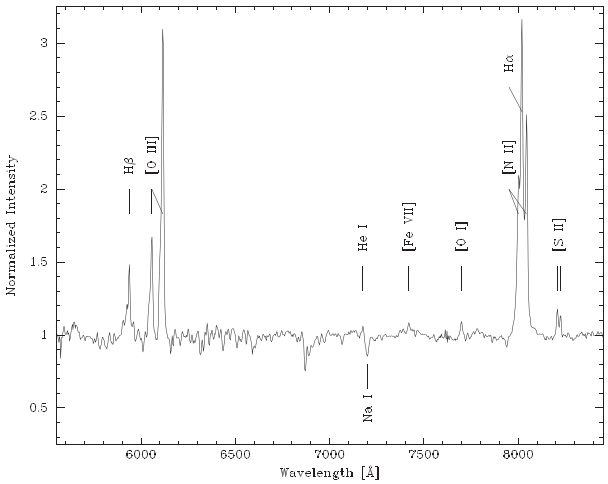

Figure 4. Gemini-GMOS spectrum of the nuclear region of the optical counterpart of 3XMM J005450.3–373849. Prominent emission and absorption lines are indicated.

opposite sides of the nucleus, are associated with strong ongoing star formation, as is the case of other well-studied starburst galaxies (e.g. M 94; Waller et al. 2001).

ACKNOWLEDGEMENTS

We thank the anonymous referee for her/his insightful comments and constructive suggestions that led to an improved manuscript. JAC is a CONICET researcher. This work was supported by Consejería de Economía, Innovación, Ciencia y Empleo of Junta de Andalucía under excellence grant FQM-1343 and research group FQM-322, as well as FEDER funds. MJR was supported by grant PIP 112-201101-00301 (CONICET). RG was supported by grant PIP 112-201201-00298 (CONICET). FG and MJR are fellows of CONICET.

REFERENCES

Arnaud K. A., 1996, ASP Conf. Ser. 101. Astronomical Data Analysis Software and Systems V. Astron. Soc. Pac., San Francisco, p. 17
Balucinska-Church M., McCammon D., 1992, ApJ, 400, 699
Bresolin F., Pietrzyński G., Gieren W., Kudritzki R.-P., 2005, ApJ, 634, 1020
Buta R., Crocker D. A., 1991, AJ, 102, 1715
Cappi A., Held E. V., Marano B., 1998, A&AS, 129, 31
Carpano S., Wilms J., Schirmer M., Kendziorra E., 2005, A&A, 443, 103
Cisternas M., Sheth K., Salvato M., Knapen J. H., Civano F., Santini P., 2015, ApJ, 802, 137
Collins C. A., Guzzo L., Nichol R. C., Lumsden S. L., 1995, MNRAS, 274, 1071
Dalcanton J. J. et al., 2009, ApJS, 183, 67
Dolphin A. E., 2000, PASP, 112, 1383
Fabbiano G., 2006, ARA&A, 44, 323
Foight D., Guver T., Ozel F., Slane P., 2015, preprint (arXiv:1504.07274)
Gieren W. et al., 2004, AJ, 128, 1167
Hunt L. K., Malkan M. A., 1999, ApJ, 516, 660
Merloni A. et al., 2014, MNRAS, 437, 3550
Mushotzky R. F., Done C., Pounds K. A., 1993, ARA&A, 31, 717
Payne J. L., Filipović M. D., Pannuti T. G., Jones P. A., Duric N., White G. L., Carpano S., 2004, A&A, 425, 443
Read A. M., Pietsch W., 2001, A&A, 373, 473
Rosen S. R. et al., 2015, preprint (arXiv:1504.07051)
Schirmer M., Erben T., Schneider P., Pietrzynski G., Gieren W., Carpano S., Micol A., Pierfederici F., 2003, A&A, 407, 869
Schwarz M. P., 1981, ApJ, 247, 77
Strüder L. et al., 2001, A&A, 365, L18
Turner M. J. L. et al., 2001, A&A, 365, L27
Ueda Y., Akiyama M., Hasinger G., Miyaji T., Watson M. G., 2014, ApJ, 786, 104
Waller W. H. et al., 2001, AJ, 121, 1395
Weedman D. W., 1977, ARA&A, 15, 69
Wright E. L., 2006, PASP, 118, 1711

This paper has been typeset from a TEX/LATEX file prepared by the author.